Development of Advanced Hydride Reorientation Model and Experimental Validation

Changhyun Jo, Youho Lee*
Department of Nuclear Eng., Seoul National Univ., 1 Gwanak-ro Gwanak-gu, Seoul 08826, Republic of Korea
**Corresponding author: leeyouho@snu.ac.kr*

***Keywords : hydride reorientation, thermodynamic modeling, EBSD characterization**

1. Introduction

During normal operation, hydrogen generated by oxidation is absorbed into the cladding and precipitates as hydrides during dry storage. If tensile hoop stress is applied, hydride reorientation may occur, leading to significant degradation. Hydride reorientation is influenced by various factors such as microstructure, hydrogen content, hoop stress, and temperature profile, which evolve over the long period from fabrication to dry storage.

Numerous studies have been conducted on hydride reorientation modeling, yet the results often diverge from experimental observations due to bold and unsafe assumptions regarding microstructural information. However, recent advancements in Electron Backscatter Diffraction (EBSD) technology have enabled successful characterization of reactor-grade cold worked stress relieved (CWSR) zirconium cladding, leading to new findings. Notably, it has been discovered that radial and circumferential hydrides exhibit similar aspect ratios and misfit strains. These observations have propelled advancements in reorientation modeling.

This study is dedicated to developing a thermodynamic model for hydride reorientation. It calculates the nucleation rate for radial and circumferential hydride utilizing classical nucleation theory with microstructural information attained by EBSD characterization. The model is coupled with the hydride-nucleation-growth-dissolution (HNGD) model [1], which captures transient hydride precipitation behavior, allowing for a quantitative examination of reorientation behavior. Validation of the model has been performed using experimental results across a wide range of hydrogen concentrations, cooling rates, and stress conditions.

2. Experimental setup

2.1. Hydrogen charging

Before hydride reorientation, un-irradiated reactor-grade CWSR Zr-Nb1% claddings were charged with hydrogen in the vessel. Hydrogen gas was injected into the vessel at 400°C, where it dissolved into the specimens as the vessel pressure decreased. Various hydrogen concentrations were achieved by adjusting the pressure drop.

2.2. Hydride reorientation

The hydride reorientation tests were conducted using the hydride reorientation system, as illustrated in **Fig. 1**. To prevent any potential leaks during experiments, an appropriately sized cap was utilized to seal the end of the hydrogen-charged cladding tube. This tube was then inserted into the pressurization tubes within the radiant furnace. The external environment of the tube was evacuated using a vacuum pump, and the temperature was gradually increased to the target level of 400°C using an electric heater. Once the temperature reached 400°C, internal pressurization was achieved by introducing Argon gas, generating multi-axial stress in the cladding tube throughout the cooling process. To monitor the cladding temperature throughout the process, three thermocouples were affixed to the surface of the tube.

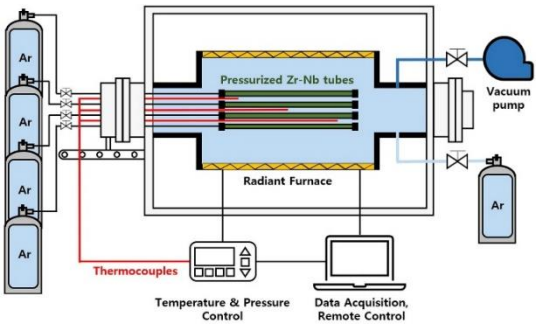

Fig. 1. Hydride reorientation apparatus [2]

The hydride-reoriented specimens were cut into 7mm lengths. All sub-specimens were then polished and etched for optical microscopy (OM). The OM images were utilized to measure the radial hydride fraction (RHF) using the SNU-developed image analyzing tool, PROPHET [3], which automatically detects hydrides and calculates the RHF of the input image. Additionally, hydrogen concentration was measured using ELTRA ONH-2000.

3. Model development

3.1. Theoretical backgrounds

In reactor-grade CWSR cladding, most hydrides are precipitated at grain boundaries due to small grain and high energetic incentives [4]. During precipitation, chemical stabilization and elimination of grain boundary (GB) occurs, inducing local stress and strain fields around the precipitates and forming new interfaces

between zirconium and hydrides. For precipitation to occur, the hydride must overcome the critical nucleation energy (ΔG^*), as defined by **Eq. 1**, which can be derived from the differentiation of Gibbs free energy change.

$$(1)\ \Delta G^* = \frac{16\pi\sigma_{\alpha\delta}^3}{3(-\Delta G_{chem} + \Delta G_{strain})^2} f$$

$$with\ f = 1 - 1.5cos\psi + 0.5\cos^3\psi$$

where ΔG_{chem} and ΔG_{strain} are chemical and strain energy change, respectively, $\sigma_{\alpha\delta}$ is interfacial energy between zirconium and hydride, ψ is $\cos^{-1}(\sigma_{\alpha\alpha}/2\sigma_{\alpha\delta})$, $\sigma_{\alpha\alpha}$ is GB energy.

Furthermore, the critical nucleation energy can be directly converted into a kinetic parameter, the nucleation rate, using a simple Arrhenius function (**Eq. 2**).

$$(2)\ J^* = Z\beta^* N exp\left(-\frac{\Delta G^*}{RT}\right)$$

where Z is zeldovich factor, β^* is rate at which atoms or molecules are added to the critical nucleus, N is nucleation site density.

By dividing the nucleation rate at radial GB with circumferential one, nucleation rate ratio can be determined (**Eq. 3**), which represents the relative magnitude of radial hydride precipitation. Nucleation rate ratio plays a key role of determining orientation assignment in the model

$$(3)\ \frac{J_{rad}^*}{J_{circ}^*} = \frac{(Z\beta^* N)_{rad}\, exp\left(-\frac{\Delta G_{rad}^*}{kT}\right)}{(Z\beta^* N)_{circ}\, exp\left(-\frac{\Delta G_{circ}^*}{kT}\right)}$$

The free energy changes included in **Eq. 1** are derived from reasonable physical backgrounds. If the stress induced by the misfit and enthalpic effects are neglected, the chemical free energy can be expressed by bulk solubility limit, TSS_P and TSS_d. However, in reality, significant stress is induced in the matrix due to the volume expansion of precipitate. Therefore, a simple Arrhenius function with constant A and ΔP_h is introduced to relate the bulk solubility to near field solubility considering stress and enthalpic effects.

$$(4)\ \Delta G_{chem} = \frac{xRT}{\bar{V}_{hyd}} \ln\left(\frac{TSS_p}{TSS_d} \times Aexp\left(\frac{\Delta P_h \bar{V}_h}{RT}\right)\right)$$

Due to the lattice misfit and volumetric change, precipitate causes alterations in atom arrangements within the matrix, leading to the accommodation of strain energy. From the EBSD result indicating the incoherent interface between zirconium and hydride, strain energy is determined by volumetric strain rather than lattice misfit strain [5]. Since the applied stress slightly modifies the strain energy, the interaction energy (=$-\boldsymbol{\chi\bar{\omega}}$) is included in the formula.

$$(5)\ \Delta G_{strain} = \frac{2}{3}\mu\Delta^2 f\left(\frac{c}{a}\right) - \chi\bar{\omega}$$

where μ is shear modulus, Δ is volumetric strain, c/a is hydride aspect ratio, $\bar{\omega}$ is applied tensile stress, χ is misfit strain along tensile stress. Since the order of magnitude of interaction energy is ~ 0.01 of the total strain energy, volume expansion(Δ) and hydride morphology (c/a) play an important role for strain energy.

Intergranular hydrides, predominantly observed in CWSR cladding, eliminate the GBs and form new interfaces, leading to alert in Gibbs free energy change, which is reflected in interfacial energy ($\sigma_{\alpha\delta}$) and shape function *f*. If the tensile stress is applied to the GBs, local strains increase, leading to an elevation of grain boundary energy ($\sigma_{\alpha\alpha}$). Since the hoop stress is dominant in cladding geometry, radial GBs are highly activated and become favorable nucleation site, arising from the high energetic incentive from eliminating GBs (**Eq. 6**),

$$(6)\ \sigma_{\alpha\alpha,rad} = \sigma_{\alpha\alpha,circ} + k_{GB}\sigma_h$$

where $\sigma_{\alpha\alpha}$ is GB energy, σ_h is hoop stress, k_{GB} is a constant relates $\sigma_{\alpha\alpha}$ and σ_h.This is the primary driving mechanism that overcomes the spatial disadvantage of circumferentially elongated grain structure.

3.2. Employed parameters

Some parameters had been quantified through EBSD observation : nucleation site density (N), hydride aspect ratio (c/a). $\boldsymbol{N_{rad}/N_{circ}}$ was directly replaced by grain boundary length ratio due to the circumferentially elongated grain morphology, as shown in **Fig. 2**. Hydride aspect ratio is slightly higher for radial hydrides, as shown in **Fig. 3**.

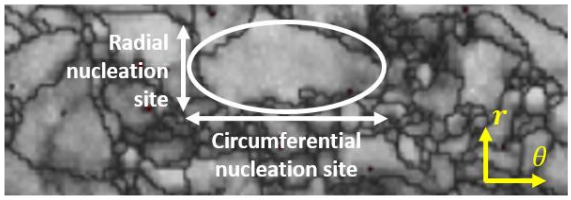

Fig. 2. Elongated Zr grain morphology (EBSD)

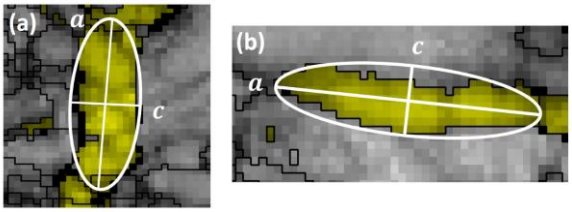

Fig. 3. Hydride morphology (EBSD)

Meanwhile, interfacial energies ($\sigma_{\alpha\delta}$, $\sigma_{\alpha\alpha}$) were selected within a reasonable ranges of ~$\mathbf{0.1\ J/m^2}$, while the k_{GB}, A, ΔP_h were chosen to best fit the experimental results.

3.3. Coupling with HNGD model

To quantitatively analyze the reorientation behavior, developed thermodynamic model is coupled with HNGD model, which represents the transient precipitation behavior. At each time step, the model calculates the nucleation and growth amount. Nucleation refers to creating new nuclei by overcoming energy barrier, while growth refers to growth of pre-existing nuclei due to stress concentration at hydride tip. Subsequently, the orientation is assigned to the determined precipitation amount using the following methods: For the nucleation, the distribution is proportional to nucleation rate, as discussed in **Sec. 3.1**. For the growth, the distribution is proportional to the number density of precipitated hydrides up to the current time step.

Fig. 4 provides an overview of integrated radial hydride precipitation model. Given the input parameters of hydrogen concentration, temperature and hoop stress profile, the combined structure is iterated over time to calculate the final RHF.

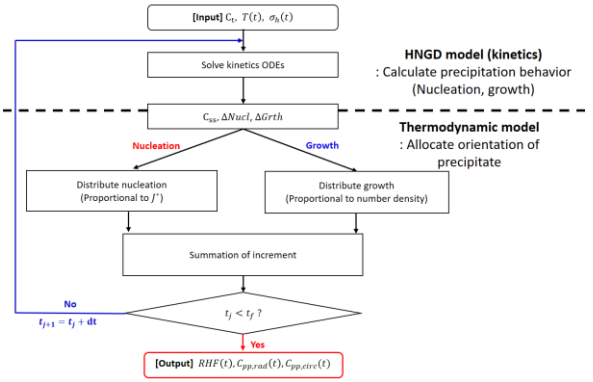

Fig. 4. Schematic of the reorientation model

3.4. Validation

Hydride reorientation apparatus shown in **Fig. 1** was used to validate the thermodynamic model. Experimental conditions are summarized in **Table 1**.

Table 1. Summarized experimental conditions

Variables	Range
H content	60 ~ 570 wppmH
Cooling rate	0.067~3℃/min
Internal pressure (hoop stress)	10 ~ 20 MPa (78~157 MPa)

As illustrated in **Fig. 5**, the model demonstrates high predictability for RHF compared to the measured RHF by PROPHET, However, deviations are observed in fast cooling scenarios, where the system strays from equilibrium, making the application of thermodynamics less appropriate.

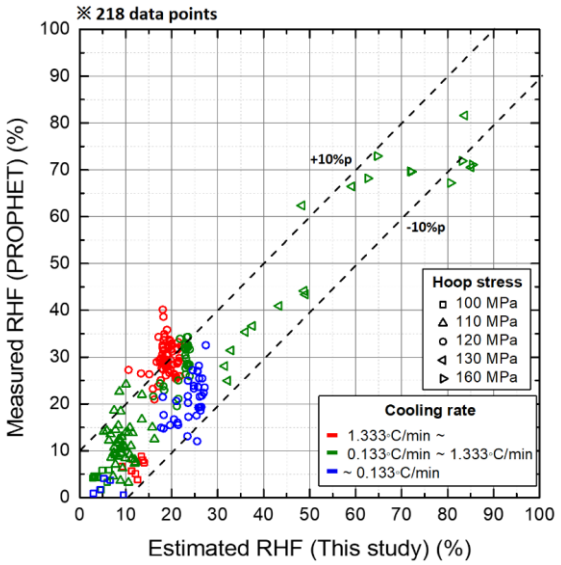

Fig. 5. Model-to-Experimental comparison of RHF

4. Sensitivity study

Variable sensitivities on hydride reorientation have been investigated using the developed model.

4.1. Hoop stress

Fig. 6 shows hoop stress effect on reorientation. The RHF increases with higher hoop stress applied during cooling, rapidly soaring beyond a certain threshold. This threshold value closely approaches the current US NRC regulation limit of 90MPa.

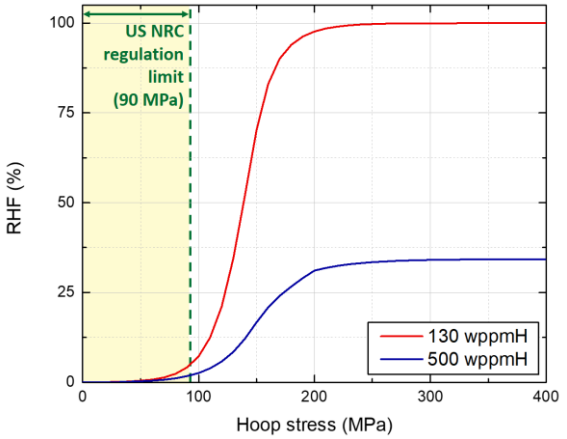

Fig. 6. Hoop stress effect on reorientation

4.2. Hydrogen concentration

The effect of hydrogen concentration on reorientation can be categorized into two ranges, as depicted in **Fig. 7**. For the concentration below the solubility limit of peak temperature, RHF increases due to the increased

nucleation at high temperature, which is favored for radial hydride precipitation. However, above the solubility limit, RHF decreases with increasing hydrogen concentration as all undissolved hydrides at peak temperature remain in the circumferential orientation. Consequently, the RHF peak is situated at the solubility limit at peak temperature. It is noteworthy that strong hoop stress may slightly shift the RHF peak to the left.

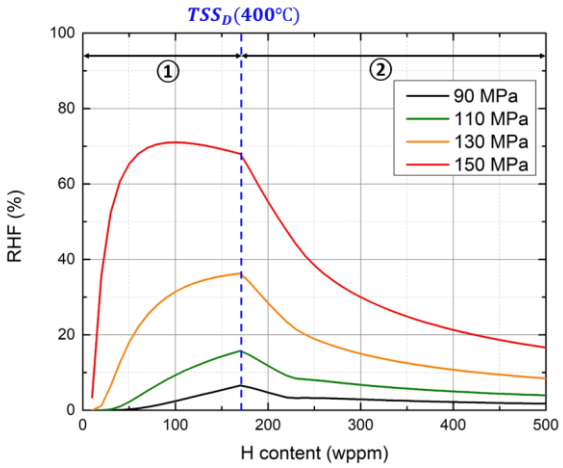

Fig. 7. Hydrogen concentration effect on reorientation

4.3. Cooling rate

Cooling rate effect varies depending on the hoop stress. Under typical dry storage conditions of 90MPa, as shown in **Fig. 8**, RHF increases with a slower cooling rate. It arises from increased nucleation at higher temperatures during early stages of cooling. However, for the extreme condition of 150MPa in **Fig. 9**, RHF slightly decreases with a slower cooling rate because of the growth of pre-existing circumferential hydrides, while the hoop stress effect on nucleation is being high enough over the wide range of temperatures.

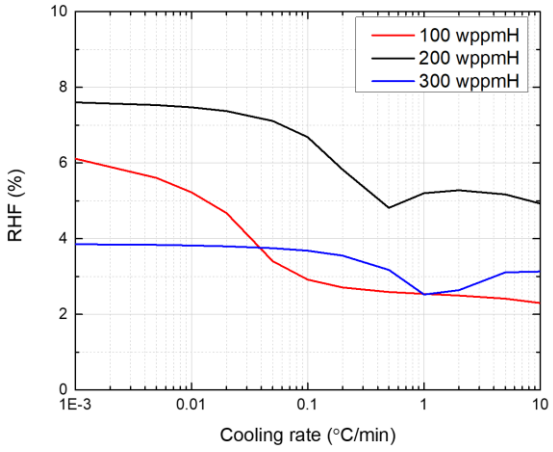

Fig. 8. Cooling rate effect on reorientation for 90MPa hoop stress

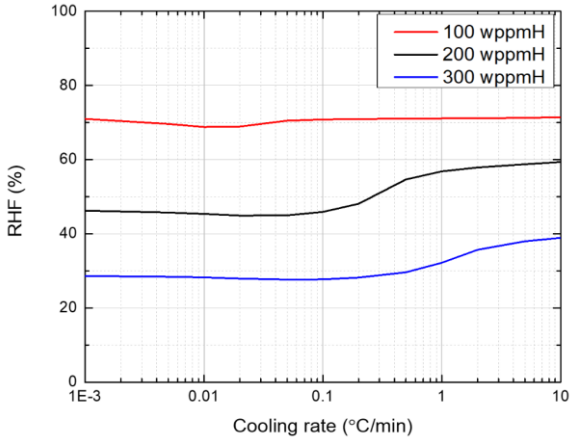

Fig. 9. Cooling rate effect on reorientation for 150MPa hoop stress

5. Conclusion

An advanced thermodynamic model for hydride reorientation has been developed utilizing the radial GB segregation effect as the primary driving mechanism for reorientation. It quantitatively evaluates the RHF for given inputs of hydrogen content, pressure and temperature profiles. The model has been validated with wide ranges of experimental data and exhibits high accuracy by incorporating the realistic microstructure captured by EBSD characterization. Furthermore, it effectively captures the key sensitivities on reorientation.

ACKNOWLEDGEMENT

This work was supported by the Institute of Korea Spent Nuclear Fuel grant funded by the Korea government the Ministry of Trade, Industry and Energy (2021040101002A).

REFERENCES

[1] F. Passelaigue, E. Lacroix, G. Pastore, and A. T. Motta, Implementation and validation of the hydride nucleation-growth-dissolution (HNGD) model in BISON. *Journal of Nuclear Materials* 544 (2021): 152683.

[2] D. Woo, Y. Lee, Understanding the mechanical integrity of Zircaloy cladding with various radial and circumferential hydride morphologies via image analysis. *Journal of Nuclear Materials* 584 (2023): 154560.

[3] D. Kim, D. Kim, D. Woo, Y. Lee, Development of an image analysis code for hydrided Zircaloy using Dijkstra's algorithm and sensitivity analysis of radial hydride continuous path. Journal of Nuclear Materials 564 (2022): 153647.

[4] D, Woo, J. Kang, Y. Lee, Advanced microstructural characterization of circumferential and radial hydrides in reactor-grade Zirconium cladding tube using EBSD and DSC, 2023 ANS Winter Conference and Expo.

[5] D. A. Porter, K. E. Easterling, M. Y. Sherif, Phase transformations in metals and alloys, Garland Science, 2010. pp. 142, 2021.